

Article

# Decoupling Design and Verification of a Free-Piston Linear Generator

Peng Sun <sup>1,2</sup>, Chi Zhang <sup>1,\*</sup>, Jinhua Chen <sup>1</sup>, Fei Zhao <sup>1</sup>, Youyong Liao <sup>1</sup>, Guilin Yang <sup>1</sup> and Chinyin Chen <sup>1</sup>

<sup>1</sup> Ningbo Institute of Materials Technology & Engineering, Chinese Academy of Sciences, Zhejiang Key Laboratory of Robotics and Intelligent Manufacturing Equipment Technology, Ningbo 315201, China; sunpeng@nimte.ac.cn (P.S.); chenjinhua@nimte.ac.cn (J.C.); zhaofei@nimte.ac.cn (F.Z.); liaoyy@nimte.ac.cn (Y.L.); glyang@nimte.ac.cn (G.Y.); chenchinyin@nimte.ac.cn (C.Y.)

<sup>2</sup> University of Chinese Academy of Sciences, Beijing 100049, China

\* Correspondence: zhangchi@nimte.ac.cn; Tel.: +86-574-8666-9754

Academic Editor: K.T. Chau

Received: 7 September 2016; Accepted: 8 December 2016; Published: 16 December 2016

**Abstract:** This paper proposes a decoupling design approach for a free-piston linear generator (FPLG) constituted of three key components, including a combustion chamber, a linear generator and a gas spring serving as rebounding device. The approach is based on the distribution of the system power and efficiency, which provides a theoretical design method from the viewpoint of the overall power and efficiency demands. The energy flow and conversion processes of the FPLG are analyzed, and the power and efficiency demands of the thermal-mechanical and mechanical-electrical energy conversion are confirmed. The energy and efficiency distributions of the expansion and compression strokes within a single stable operation cycle are analyzed and determined. Detailed design methodologies of crucial geometric dimensions and operational parameters of each key component are described. The feasibility of the proposed decoupling design approach is validated through several design examples with different output power.

**Keywords:** free-piston; linear generator; decoupling design; power and efficiency distribution

## 1. Introduction

The free-piston linear generator (FPLG) is a novel energy converter with advantages of high efficiency, high power density, and low emissions. Due to the elimination of the crankshaft and flywheel mechanism, the compression ratio of FPLG is variable. This provides an attractive option to accommodate multiple fuels, like the diesel, gasoline, ethanol, hydrogen, methane, natural gas and so forth, without modifying the mechanical configuration of the combustion engine. Therefore, the FPLG is regarded as a promising alternative hybrid power system for hybrid electrical vehicles (HEVs) [1–5].

Although the elimination of the crankshaft and flywheel brings many advantages to the FPLG, it also poses challenges for stable operation. The piston motion of the FPLG is determined by the total forces acting on the piston-rod, in which the expansion force generated by the combustion, the electromagnetic force of the linear electric machine (LEM) and the rebounding force of the gas spring (GS) are the dominant forces. The combustion fluctuation results in the variation of the expansion force, and hence leads to cycle-to-cycle variations of the motion states of the free-piston. Once the piston cannot reach the top dead center (TDC) position, the combustion of the following cycles will be insufficient, which will thereby cause unstable operation [6].

Many investigations have been conducted since the first FPLG concept was proposed by the Canadian researcher Kos in the 1990s [6]. The researched FPLGs can be generally classified into single-cylinder, dual-piston and the opposed-piston types [1]. For single-cylinder FPLGs, a rebounding mechanism like a gas spring, mechanical spring, or a hydraulic actuator is necessary.

Many institutions, such as the German Aerospace Centre (DLR), Toyota Central R & D Labs Inc. (Toyota), and the Nanjing University of Science and Technology (NUST), have carried out abundant studies on single-cylinder FPLGs. Kock et al. at DLR developed a two-stroke single-cylinder FPLG with the gas spring functioning as a rebounding device [7–10]. The test data showed that it could produce an electric power output of roughly 10 kW at 21 Hz. The output power could be further improved up to 25 kW by increasing the motion frequency up to 50 Hz. Kosaka et al. in Toyota also developed a two-stroke gas spring rebounded single-cylinder FPLG prototype [11,12]. The piston was specially designed to be a W-shaped structure, which was beneficial for long-duration operation because it could prevent the magnet from demagnetizing as a result of heating. It was reported the FPLG could realize continuous operation lasting about four hours, which could provide 10.4 kW power output with the overall efficiency of 36.2%. Xu and Chang at NUST developed a four-stroke prototype with mechanical spring rebounding. The linear electric machine was designed to be a moving-coil DC voice coil motor (VCM). The average output power was only 2.2 kW with the generating efficiency of 32% [13,14].

The dual-piston type FPLG is a common configuration that has been widely studied by many institutions such as the Royal Institute of Technology (KTH), West Virginia University (WVU), Shanghai Jiao Tong University (SJTU), Newcastle University and the Beijing Institute of Technology (BIT). Hansson et al. at KTH [15–17] developed a dual-piston FPLG prototype. The rated power of the generator was near 29 kW. The mean system efficiency is 23%. Their work mainly focused on the optimization design of the linear electric machine specifically used in FPLG. Shoukry et al. at WVU established a dual-piston two-stroke prototype, which could produce a peak output electric power of 316 W with a frequency of 23.1 Hz [18–20]. Xiao et al. at SJTU have also studied the dual-piston FPLG. They also developed a prototype and the motion characteristics of the prototype were thoroughly investigated [21].

Mikalsen et al. at Newcastle University have carried out systematical studies focusing on the dual-piston FPLG configuration, including the design, modeling, thermodynamics modeling and control strategies [22–28]. More recently, Roskilly in cooperation with Jia et al. at BIT [29–31] developed a two-piston prototype that was estimated to have the potential of producing 3.76 kW electric power with an efficiency of 34.5% [31–38].

There are also a few studies on opposed-piston FPLGs. Van Blarigan et al. at Sandia National Laboratory (SNL) developed an opposed-piston prototype. Their goal was to design a 30 kW FPLG as the fuel cell for a hybrid electric vehicle (HEV) [39,40]. The synchronous control of the opposed-piston FPLG is relatively more difficult than the single-piston and dual-piston types.

From the previous research works, we can find that with the single-cylinder FPLG is easier to realize stable operation control compared with the dual-piston and opposed-piston types. Therefore the single-piston FPLG with gas spring rebounding device is regarded as one of the most promising designs [3,7]. However, the long-time stable operation of the single-cylinder FPLG is still a challenging problem. Besides lacking effective control strategies, improper system design can also lead to unstable operation.

The design of a single-cylinder FPLG is relatively more complex because of the implementation of the gas spring. There are a few references that specifically study system design approaches for FPLGs. Schneider et al. introduced some design considerations of the power and efficiency demands for different package concepts of the FPLG used for HEVs. They also analyzed the energy losses and efficiency distribution of the FPLG system. The power profile with respect to the velocity was presented and simulated [10]. Roskilly et al. analyzed the effects of operational variables on the overall performance of the FPLG and gave several design considerations such as the engine configuration,

the control objectives, moving mass, compression ratio, exhaust back pressure and so forth are essential for the design [25–28]. Smallbone et al. designed and simulated a two-stroke and four-stroke FPLG. The system model was established and analyzed, however a detailed design approach was not introduced [32]. Mao et al. proposed a method of parameters coupling design of diesel FPLG based on the energy conservation relationship. In order to define the main geometric dimensions, an iterative procedure was carried out among the zero-dimensional numerical simulation, Computational Fluid Dynamics (CFD) calculation of the gas exchanging process and the combustion process [41].

Kleemann et al. studied a computational design methodology for a FPLG [42]. It was based on the computational design optimization for a two-stroke two-cylinder FPLG. Iterations between zero-dimensional, one-dimensional and simplified CFD models were utilized to define the operating conditions and overall geometrical parameters. In addition, more detailed three-dimensional CFD calculations have been used to optimize the configurations of the internal combustion engine (ICE). Mao et al. proposed a similar method of parameters coupling design of a diesel FPLG. In order to determine the main structural dimensions, an iterative procedure was carried out using zero-dimensional numerical simulation, CFD calculation of the gas exchanging process and the combustion process [41]. These two design methodologies are actually a kind of coupled design approach that needs a large number of iterative calculations, and also needs rich experimental knowledge, especially for FPLG systems. They are not theoretical and universal design approaches. What's more, during the coupled design process mentioned above, some of the performance demands, structural and operational parameters of the major components are coupled together and must be predefined at the same time and be determined through interactive computation. It always makes the design process cumbersome.

From a different perspective, in consideration of overcoming the inconveniences of the coupled design method, we propose a decoupling design approach, which avoids the cumbersome iterative calculations and only needs a few practical predefined constraints and some empirical knowledge. The whole design is a completely top-to-down design process that only involves three major procedures. Firstly, simply from the system overall power and efficiency demands, the performance demands like the power and efficiency of each key components can be directly determined according to the energy conversion and flow. Secondly, the energy and efficiency distribution, or the converted energy and corresponding conversion efficiency of each stroke cycle during one single piston motion cycle can be determined. Combining the two steps above, the system overall performance demands can be easily assigned to each key component, so that we can design each key component independently without any iterations. Thereby, we can determine the structural and operational parameters of each component based on certain mechanical constraints and a few empirical pre-definitions.

The feasibility of the proposed design approach was verified and simulated through several design examples of various power-level demands under different motion frequency (10 kW @ 20 Hz, 15 kW @ 25 Hz, 20 kW @ 30 Hz, 25 kW @ 30 Hz) conditions. Importantly, the proposed decoupling design is a theoretical and universal approach. It can not only be applied for designing a single-cylinder FPLG with gas spring, mechanical spring or hydraulic rebounding device, but can also be used for designing a dual-piston FPLG.

## 2. Decoupling Design of a Free-piston Linear Generator (FPLG) System

The structure illustration of the FPLG studied in this work, which consists of a gas spring (GS), a linear electric machine (LEM) and an internal combustion engine (ICE) is shown in Figure 1. The GS acts as a rebound device. The LEM mover is driven reciprocally to generate electrical power through the coupled consequence of the periodical combustion expansion in the LEM cylinder and GS rebounding.

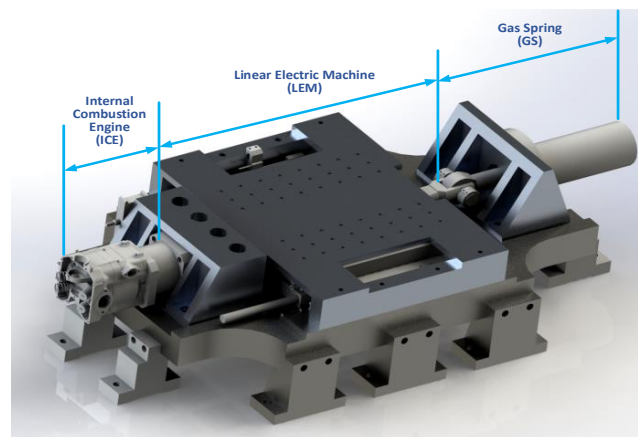


**Figure 1.** The 3D structure of a FPLG.

The proposed decoupling design process can be divided into three phases:

- I. To decide the power and efficiency demands of thermal-mechanical and mechanical-electrical energy conversions from the design specifications based on the energy flow and conversion processes.
- II. To determine the energy and efficiency distribution of the expansion and compression strokes within a single operation cycle according to the output electrical power profile.
- III. To choose appropriate structural and operational parameters of the key components that satisfies the power and efficiency specifications.

The proposed decoupling design process can be summarized as in Figure 2.

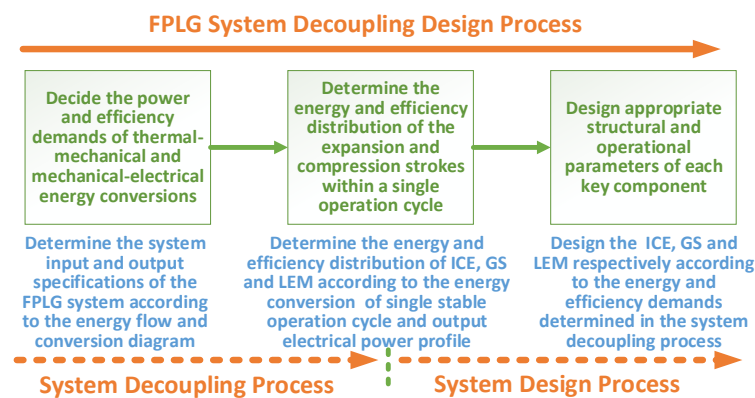


**Figure 2.** Proposed decoupling design process of FPLG system.

In order to illustrate the proposed decoupling design approach in details, we take a 25 kW FPLG design as an example according to the New European Driving Cycle (NEDC) [10]. The major objective design specifications are listed in Table 1.

**Table 1.** Crucial design specifications.

Nominal	Value
Effective electric power output	25 kW
Generating efficiency	94%
System overall efficiency	35.5%
Motion frequency	15–35 Hz

2.1. Power and Efficiency Demands of Energy Conversion Processes

Figure 3 shows the energy flow and conversion diagram of the FPLG system, which illustrates the energy loss and efficiency distribution from fuel chemical energy to electrical energy. Before designing a FPLG system, we must clarify the system input and output specifications.

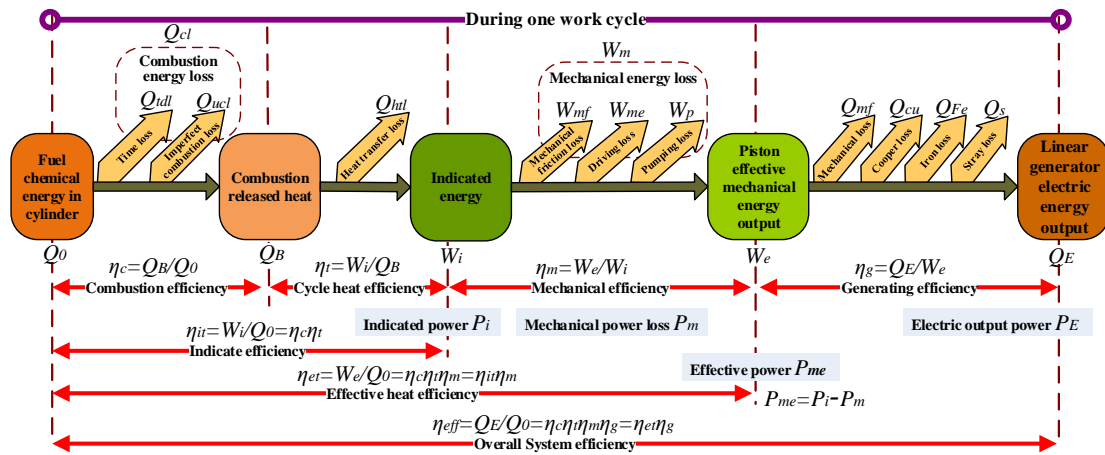


Figure 3. System energy flow diagram.

In Figure 3,  $Q_0$  represents the total chemical energy of the fuel in the cylinder,  $W_e$  is the net effective mechanical energy output of the piston. Because the LEM is the core energy conversion device for the FPLG system, from the point of view of the LEM,  $W_e$  is the input and  $Q_E$  is the output. Also,  $Q_E$  is the output of the FPLG system. Considering this the thermal-mechanical energy conversion from  $Q_0$  to  $W_e$  can be regarded as the system input process. The mechanical-electrical energy conversion from  $W_e$  to  $Q_E$  can be viewed as the system output process. According to the system input specifications, the ICE and GS can be designed preliminarily. According to the system output specifications, we can initially design the LEM.

The effective electric power, overall system efficiency and generating efficiency are three major specifications that needed to be predefined. According to the New European Driving Cycle (NEDC), a 25 kW FPLG system is already sufficient for a continuous speed of about 125 km/h [10]. For a single FPLG module with gas spring, the system efficiency including all auxiliaries ranged from 31% to 33% depending on the system load. It can be increased by 1%–3% through optimizing the power used by auxiliary units [3]. The generating efficiency of PM linear electrical machine for FPLG system should be larger than 90% [43]. Typically, the tested generating efficiency of the PM linear generator for FPLG system is about 92%–94% [44]. Considering above, our design expectation is that the FPLG system can provide 25 kW effective electric output power with the overall system efficiency of no less than 35.5%. And the generating efficiency is expected to be designed as higher as possible (94% at least). Once the effective electric power, overall system efficiency and generating efficiency are determined, according to the energy flow diagram shown as Figure 3 and the design specifications shown in Table 1, the effective mechanical power of ICE and the effective heat efficiency can be calculated accordingly with the values of 26.6 kW and 37.77%. These two specifications are the significant preconditions for ICE design. The power and efficiency demands of the thermal-mechanical and mechanical-electrical energy conversions are listed in Table 2.

Table 2. Input and output power and efficiency demands.

Nominal	Value	Nominal	Value
$P_E$	25 kW	$\eta_{eff}$	35.5%
$P_{me}$	26.6 kW	$\eta_{et}$	37.77%

### 2.2. Energy and Efficiency Distribution within a Single Operation Cycle

Figure 4 describes the simplified energy distribution within each operation cycle at stable operation.

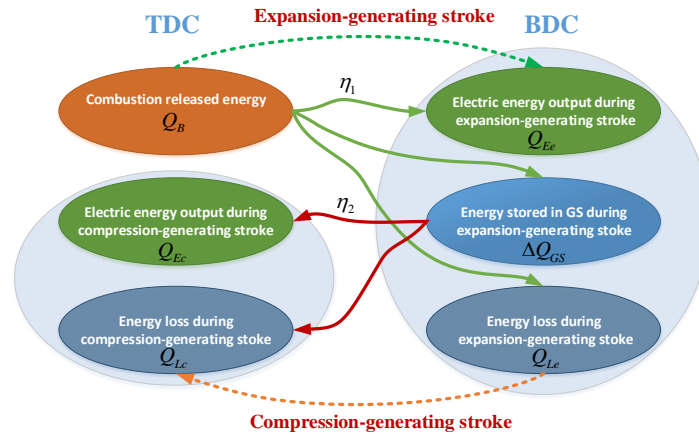


Figure 4. Simplified energy distribution of each operation cycle at stable operation.

During the expansion-generating stroke, the piston is driven from its top dead center (TDC) to bottom dead center (BDC). In this process, part of the combustion released energy  $Q_B$  is converted into electrical energy  $Q_{Ee}$  with the expansion-generating efficiency  $\eta_1$ , and another part is stored in the GS in the form of elastic potential energy  $\Delta Q_{GS}$  that will be released in the next compression-generating stroke.  $Q_{Le}$  represents the energy loss in the expansion-generating stroke, including the combustion energy loss, the heat transfer loss, the mechanical energy loss and the LEM loss.

During the compression-generating stroke, the piston is rebounded from BDC to TDC mainly by the energy stored in GS. Part of  $\Delta Q_{GS}$  is converted into energy  $Q_{Ec}$  with the compression-generating efficiency  $\eta_2$ . Similarly,  $Q_{Lc}$  represents the energy loss in the compression-generating stroke, mainly including the friction loss and LEM generating loss. Correspondingly, the profile of the output electrical power of each operation cycle is shown in Figure 5.

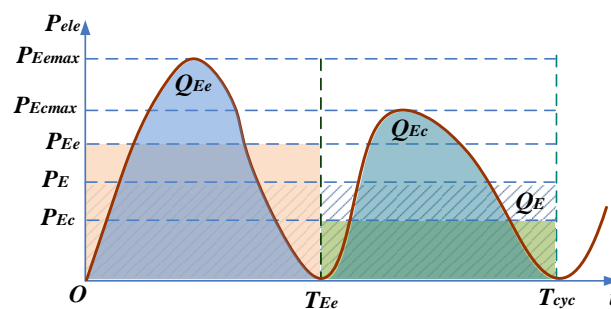


Figure 5. Electric power output of each operation cycle.

In order to satisfy the specifications of the power and efficiency, the point of design phase II is to determine the energy distribution, the power profile and the conversion efficiency according to Figures 4 and 5. Assuming each stroke lasts for the same duration, and the motion cycle duration is  $T_{cyc}$ , it is easy to get the following equations:

$$Q_{Ee} = \int_0^{\frac{T_{cyc}}{2}} P_{ele} dt = \frac{1}{2} P_{Ee} T_{cyc} = \eta_1 Q_B \tag{1}$$

$$Q_{Ec} = \int_{\frac{T_{cyc}}{2}}^{T_{cyc}} P_{ele} dt = \frac{1}{2} P_{Ec} T_{cyc} = \eta_2 \Delta Q_{GS} \quad (2)$$

$$Q_E = Q_{Ee} + Q_{Ec} = \int_0^{T_{cyc}} P_{ele} dt = P_E T_{cyc} = \frac{\eta_{eff}}{\eta_c} Q_B \quad (3)$$

From (1)–(3), we get:

$$\frac{\Delta Q_{GS}}{Q_B} = \frac{\eta_{eff} - \eta_1 \eta_c}{\eta_c \eta_2} \quad (4)$$

Assuming that:

$$Q_{Ee} = k Q_{Ec} \quad (5)$$

where  $k$  is an energy difference factor between the expansion-generating stroke and compression-generating stroke, which highly depends on the characteristic of the rebound device and  $k > 1$ .

From (1), (2) and (5), we obtain:

$$\frac{\Delta Q_{GS}}{Q_B} = \frac{\eta_1}{k \eta_2} \quad (6)$$

From (4) and (6), the relationship of the efficiency distribution is derived as:

$$\eta_1 = \frac{k \eta_{eff}}{(k+1) \eta_c} \quad (7)$$

Because the friction loss of the free-piston is negligibly small, the compression-generating efficiency is hence close to the LEM generating efficiency:

$$\eta_2 \approx \eta_g \quad (8)$$

And the system efficiency can be calculated by:

$$\eta_{eff} = \frac{\eta_c P_E T_{cyc}}{Q_B} \quad (9)$$

The output electric power is approximately proportional to the square of the velocity in each stroke. It is hard to determine a precise value of the piston velocity simply through a forward-direction design process. Actually, the piston velocity is directly dependent on the stroke length and motion frequency, and it varies with the change of the injected fuel mass per cycle and also with any load changes. What's more, the piston velocity can be regulated by controlling the ICE and LEM, and the peak velocity must meet the demands of the mechanical guiderail of the LEM. Considering the above, the determination of the piston velocity needs comprehensive consideration. However, we can give an acceptable value as our design limit referencing similar design specifications and empirical data [12,22,24]. In this work, the velocity is expected to be no higher than 12 m/s in the expansion-generating stroke, and less than 7 m/s in the compression-generating stroke. Therefore, the electric energy during expansion-generating stroke is about three times that of the compression-generating stroke. Thus, we can initially define  $k = 3$ . What should be emphasized is that the peak velocity is simply our design expectation. It is just an acceptable empirical value and it is not unmodifiable. In other words, this is not the only choice set. Any other reasonable predefine is of course allowable. It has no essential effect on the feasibility validation of the proposed design approach.

Shown as Figure 3, the combustion efficiency is defined to be the ratio of the combustion released heat  $Q_B$  to the total fuel chemical energy  $Q_0$ . The combustion energy loss mainly includes the time loss and the incomplete combustion loss. The time loss is mainly caused by the combustion duration that is negligibly small. The incomplete combustion loss is mainly a result of the unburnt fuel that cannot participate in the combustion process, for example, some fuel would be attached on the cylinder walls and contribute no energy release. This is the major source of the combustion energy loss. Because

a fraction of the fuel chemical energy is not fully released inside the engine during the combustion process, it is useful to define the concept of combustion efficiency. In practice, for spark-ignition engines, the combustion efficiency is usually in the range 95%–98% [45], and it is little affected by other engine operating and design variables, provided the engine combustion process remains stable [45]. Above all, we simply define that the combustion efficiency is 97% (compromises it ranges between 95% and 98%) considering that we adapt a spark-ignited two-stroke gasoline engine.

The combustion efficiency  $\eta_c$  is generally more than 95%. Here, we define  $\eta_c = 97\%$ . As the overall system efficiency  $\eta_{eff}$  is already determined as 35.5%, the expansion-generating efficiency  $\eta_1$  is calculated to be 27.45% based on (7), and  $\eta_2$  can be determined as 94% with (8). The electrical output power  $P_E = 25$  kW, if the motion frequency is defined as 35 Hz, from (3), the necessary combustion released energy  $Q_B$  can be determined to be 1951.7 J. Afterwards, from (4),  $\Delta Q_{GS}$  can be calculated to be 190 J. Finally, from (1) and (2),  $Q_{Ee}$  and  $Q_{Ec}$  can be obtained as 535.7 J and 178.6 J. The specifications listed in Table 3 are the essential preconditions of designing the structural and operational parameters of the ICE, LEM and GS.

**Table 3.** System power and efficiency specifications.

Nominal	Value	Nominal	Value	Nominal	Value
$Q_B$	1951.7 J	$Q_{Ee}$	535.7 J	$Q_{Ec}$	178.6 J
$\Delta Q_{GS}$	190 J	$\eta_1$	27.45%	$\eta_2$	94%
$f_m$	35 Hz	$T_{cyc}$	28.57 ms	$k$	3

### 2.3. Design of the Key Components

Figure 6 depicts the crucial structural parameters and corresponding constraint relationship, where  $D$ ,  $S$ ,  $S_c$ ,  $V_c$ ,  $V_s$  are respectively the cylinder bore, stroke length, combustion clearance, effective combustor volume and discharge capacity of the ICE, and  $D_g$ ,  $S_g$ ,  $S_{cg}$ ,  $V_g$  are respectively the bore, clearance space, stroke length and instantaneous working volume of the GS cylinder. The next design phase is to select appropriate structural and operational parameters of the key components based on the power and efficiency specifications determined above.

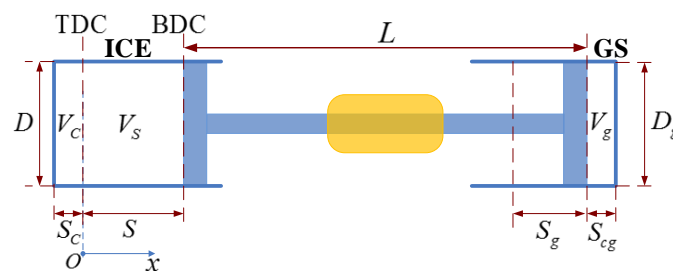


**Figure 6.** Crucial geometric parameters description of FPLG.

#### 2.3.1. Design of the Internal Combustion Engine (ICE)

According to the design specifications shown in Table 1 and the energy flow diagram shown in Figure 3, the effective mechanical output power of the ICE can be determined by:

$$P_{me} = P_E / \eta_g \quad (10)$$

where  $P_E$  is the effective electric output power, and  $\eta_g$  is the generating efficiency of LEM.

The equivalent crankshaft speed can be calculated as:

$$n_{crank} = 30 N_{strokes} f_m \quad (11)$$

where  $N_{strokes}$  is the number of strokes, and  $f_m$  is the motion frequency.

The mean velocity of the free-piston is:

$$\bar{v} = \frac{n_{crank}S}{30} \quad (12)$$

where  $S$  is the stroke length.

The discharge capacity of the ICE can be calculated by:

$$V_s = \frac{30N_{strokes}P_{me}}{N_{cylinder}n_{crank}p_{me}} = \pi \left( \frac{D}{2} \right)^2 S. \quad (13)$$

where  $N_{cylinder}$  is the number of cylinders,  $D$  is the cylinder bore,  $S$  is the stroke length,  $p_{me}$  is the mean effective in-cylinder pressure which can also be expressed as:

$$p_{me} = \frac{120N_{strokes}P_{me}}{\pi N_{cylinder}n_{crank}D^2S} \quad (14)$$

The power per liter of the ICE is:

$$P_L = \frac{P_{me}}{N_{cylinder}V_s} = \frac{p_{me}n_{crank}}{30N_{strokes}} \quad (15)$$

The ICE in this paper is a two-stroke engine with single cylinder, thus  $N_{strokes} = 2$  and  $N_{cylinder} = 1$ . As shown in Table 2, the average mechanical power  $P_{me} = 26.6$  kW. The motion frequency is expected to be 35 Hz. The mean velocity of the piston is less than 8.5 m/s. The mean effective in-cylinder pressure of a motorcycle gasoline engine lies in the range of 0.78 MPa to 1.2 MPa in general. Considering that the velocity of the free-piston is less than that of the conventional engine, the effective in-cylinder pressure of the free-piston engine is therefore lower. As a result it is designed to be 0.78 MPa. Afterwards, we can determine that the equivalent crankshaft speed  $n_{crank} = 2100$  rpm, the stroke length  $S = 120$  mm, the cylinder bore  $D = 102$  mm, and the ratio of stroke length to bore  $q_{SD} = 1.18$ . The combustion clearance space  $S_c$  is generally about 5 to 10 percent of the stroke length, i.e., 6–12 mm. In this work, it is designed to be 10 mm. The discharge capacity is 980 cc. The power per liter  $P_L = 27.14$  kW/L.

According to Figure 3, it is easy to know that the combustion heat released in each cycle can be described as:

$$Q_B = \eta_c Q_0 = H_u g_f \eta_c \chi_B \quad (16)$$

where  $H_u$  is the calorific value of fuel,  $\chi_B$  is the mass fraction burned in the combustion process and it can be described with the Weiber function as below [46,47]:

$$\chi_B = 1 - \exp \left[ -a_0 \left( \frac{t - t_0}{t_d} \right)^{b_0+1} \right] \quad (17)$$

where  $t_0$  is the ignition beginning time and  $t_d$  is the combustion duration,  $t$  is the time variable,  $a_0$  is an experimental constant and  $b_0$  is the combustion quality factor.

Thus, from (3), (16) and (17) the injected fuel mass of each cycle can be determined as:

$$g_f = \eta_c P_E T_{cyc} / \left[ \eta_{eff} H_u \left( e^{-a_0 \left( \frac{t_0}{t_d} \right)^{b_0+1}} - e^{-a_0 \left( \frac{T_{cyc}-t_0}{t_d} \right)^{b_0+1}} \right) \right] \quad (18)$$

Another key operational parameter is the initial pressure of the ICE cylinder, which is dependent on the injection mode. In this work, we employ a premixing injection mode without pressure boost. Therefore, the initial pressure of the ICE is almost the same to the standard atmospheric pressure.

Table 4 lists the specifications of the ICE obtained above.

Table 4. ICE specifications.

Nominal	Value	Nominal	Value	Nominal	Value
$D$	102 mm	$S$	120 mm	$S_c$	10 mm
$N_{strokes}$	2	$N_{cylinder}$	1	$n_{crank}$	2100 rpm
$Q_{SD}$	1.18	$V_s$	980 cc	$\eta_c$	97%
$\gamma$	1.32	$a_0$	6.908	$b_0$	2
$t_d$	4 ms	$H_u$	44,000 J/g	$p_{me}$	0.78 MPa
$P_L$	27.14 kW/L	$g_f$	45.73 mg	$p_0$	0.125 MPa

### 2.3.2. Design of the Gas Spring (GS)

The crucial geometric dimensions of the GS can also be determined based on the energy conversion relationship. Figure 7 shows the P-V diagram of the GS. At steady operation, during the expansion-generating stroke of the ICE, the GS is compressed and part of the combustion released energy  $\Delta Q_{GS}$  is stored in GS as shown in Figure 7.

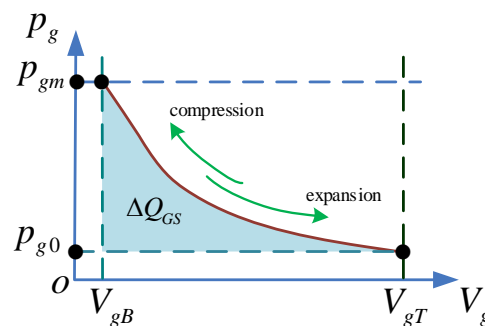


Figure 7. P-V diagram of GS.

The energy stored in GS can be calculated as:

$$\Delta Q_{GS} = \int_{V_{gB}}^{V_{gT}} (p_g - p_{g0}) dV_g = p_{meg} \pi \left( \frac{D_g}{2} \right)^2 S_g \quad (19)$$

where  $p_{meg}$ ,  $D_g$ ,  $S_g$  are the mean effective pressure, cylinder bore, stroke length of the GS, respectively,  $p_g$  and  $p_{g0}$  are the instantaneous and initial pressure in the GS cylinder,  $V_{gT}$  and  $V_{gB}$  are the instantaneous volume when the piston is respectively at its TDC and BDC positions, and  $V_g$  is the instantaneous working volume of the GS cylinder.

According to Figure 6, the stroke length of the GS equals to that of ICE, i.e.,  $S_g = S = 120$  mm. Considering the convenience of modeling analysis and manufacturing, the cylinder bore of GS is designed the same with that of ICE, i.e.,  $D_g = D = 102$  mm. Therefore, the mean effective pressure of GS  $p_{meg}$  can be calculated to be 0.2 MPa according to (19).

The pressure in the bounce chamber of the GS is significant for the compression-generating efficiency. Neglecting the stiffness regulation process and heat transferring of the GS, during compression-generating stroke, the pressure in the GS chamber can be described as:

$$dp_g = - \left( \frac{R_{gs}}{C_{vg}} + 1 \right) \frac{p_g}{V_g} dV_g = -\gamma \frac{p_g}{V_g} dV_g \quad (20)$$

where  $R_{gs}$  is the gas constant,  $C_{vg}$  is the constant-volume specific heat,  $\gamma$  is the polytropic exponent.

$$\gamma = 1 + \frac{R_{gs}}{C_{vg}} \quad (21)$$

Finally, the GS pressure can be obtained as:

$$p_g = p_{g0} \left( \frac{V_{gT}}{V_g} \right)^\gamma \tag{22}$$

This states that the pressure profile of the GS is mainly determined by the initial pressure and the instantaneous volume of the GS, which is highly depended on the piston velocity. The initial pressure of the GS can be obtained from (2), (19) and (22) as below:

$$p_{g0} = \frac{1}{2} P_{Ec} T_{cyc} \left/ \left\{ \eta_2 \left[ \frac{V_{gT}^\gamma (V_{gT}^{1-\gamma} - V_{gB}^{1-\gamma})}{1-\gamma} - (V_{gT} - V_{gB}) \right] \right\} \right. \tag{23}$$

where  $V_{gT}$  and  $V_{gB}$  are the instantaneous volume of the GS chamber when the piston is respectively at the TDC and BDC positions. Because the geometric dimensions of the GS have been confirmed,  $V_{gT}$  and  $V_{gB}$  are easy to be determined. Therefore, it is easy to know that the initial GS pressure  $p_{g0} = 0.22681$  MPa. The GS specifications obtained above are listed in Table 5.

Table 5. GS specifications.

Nominal	Value	Nominal	Value	Nominal	Value
$D_g$	102 mm	$S_g$	120 mm	$S_{cg}$	10 mm
$p_{g0}$	0.22681 MPa	$p_{meg}$	0.2 MPa	$\Delta Q_{GS}$	190 J

### 2.3.3. Design of the Linear Electrical Machine (LEM)

The LEM works as a motor to start the FPLG. Assuming that there is no burned gas in the cylinder and both the intake and exhaust valves are closed at the end of the previous stopping process. As the premixed combustion mode is adopted, the intake valve is opened (IVO) and the premixed flammable gas is sprayed into the ICE cylinder at the beginning of the starting process.

As shown in Figure 8, in the starting phase, the piston is driven from TDC to BDC by the electric motoring force, meanwhile the GS is compressed. When the piston arrives the critical starting position  $x_{sta}$ , the LEM is switched to generating mode and the piston begins to slow down. When it arrives at the scavenging position  $x_{sca}$ , the intake valve is closed (IVC). The piston is pushed towards TDC mainly by the GS rebounding force. When it reaches the igniting position  $x_{ign}$ , the first ignition starts (IGS). After that, the piston is driven by the combustion expansion force and moves towards BDC. When it reaches the scavenging position  $x_{sca}$  and the injecting position  $x_{inj}$  in sequence, the exhaust and intake valves are opened respectively (EVO and IVO).

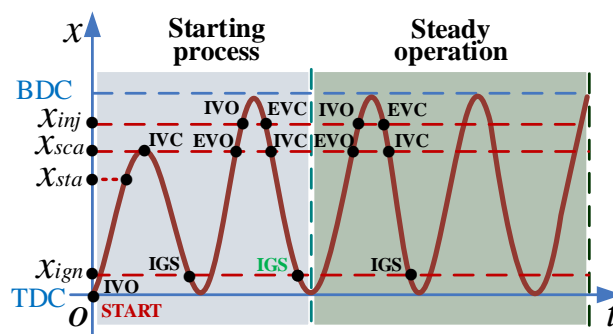


Figure 8. Starting process and steady operation illustration.

If the piston can reach the BDC position, it means that it satisfies the necessary conditions of the next ignition. When it continues moving to the positions  $x_{inj}$  and  $x_{sca}$  from BDC to TDC, the exhaust

and intake valves are closed (EVC and IVC) in order. If the piston can reach the position  $x_{ign}$  and the ICE is ignited, then the system is started successfully and it turns into steady operation. Otherwise, it needs to be started again by repeating the operations described above. According to the descriptions above, the key of successful starting is that the piston can be driven to the specific position  $x_{sta}$  with sufficient motoring force. It means that the motoring force must be larger than a certain value which can be determined from:

$$F_{Em}x_{sta} + \Delta W_p - \Delta W_{pg} - \Delta W_f \geq \Delta W_k \quad (24)$$

where  $F_{Em}$  is the effective motoring force at starting process,  $\Delta W_p$  and  $\Delta W_{pg}$  represent the work of the ICE and GS on the piston, respectively,  $\Delta W_f$  indicates the friction loss,  $\Delta W_k$  is the kinetic energy of the piston when it arrives the specific starting position  $x_{sta}$ .

There exists a minimum motoring-starting force, which can be derived from (24) as follows:

$$F_{Em} \geq \left( \int_{V_{Gsta}}^{V_{gT}} p_g dV_g - \int_{V_0}^{V_{sta}} p dV + B_v v_s x_{sta} + \frac{1}{2} M v_s^2 \right) / x_{sta} \quad (25)$$

where  $x_{sta}$  is the scavenging position,  $V_{Gsta}$  and  $V_{sta}$  are the volumes of the GS and ICE chambers when the piston is at the  $x_{sta}$  position,  $V_0$  is the initial volume of the ICE cylinder,  $v_s$  is the essential starting velocity when the piston arrives the position  $x_{sta}$ ,  $B_v$  is the friction coefficient and  $M$  is the total moving mass.

The mass of the LEM mover should be taken into consideration. The FPLG can be simply regarded as a forced vibration system with a natural frequency. Therefore there is also certain constraint among the motion frequency, the moving mass and the equivalent compression ratio, which can be described as:

$$M = \frac{K_{eq}}{(2\pi f_m)^2} \quad (26)$$

The system equivalent stiffness  $K_{eq}$  can be calculated by:

$$K_{eq} = \frac{4}{x_0^2} \frac{p_0 A}{\gamma - 1} [S_c \varepsilon_0^\gamma - (S_c + x_0) \varepsilon_p^\gamma] + \frac{4}{x_0^2} \frac{p_{g0} A_g}{\gamma - 1} [[(S_g + S_{cg}) - (S_g + S_{cg} x_0) \varepsilon_g^\gamma]] \quad (27)$$

where  $x_0$  is the equilibrium position,  $\varepsilon_0$  is the objective compression ratio,  $\varepsilon_p$  and  $\varepsilon_g$  are the compression ratios of the ICE and GS when the piston is at the equilibrium position, and:

$$x_0 = \frac{(S_g + S_{cg}) \sqrt{\gamma p_0 / p_{g0}} - S_c}{1 + \sqrt{\gamma p_0 / p_{g0}}} \quad (28)$$

$$\varepsilon_0 = \frac{S_c + S}{S_c} \quad (29)$$

$$\varepsilon_p = \frac{S_c + S}{S_c + x_0} \quad (30)$$

$$\varepsilon_g = \frac{S_g + S_{cg}}{S_g + S_{cg} - x_0} \quad (31)$$

From (26) and (27), it is concluded that the system equivalent stiffness  $K_{eq}$  is highly related to the compression ratio, the initial ICE in-cylinder pressure  $p_0$  and the initial GS pressure  $p_{g0}$ . Under a certain  $K_{eq}$ , the total moving mass should be optimized for different motion frequencies.

Figure 9 shows the relationship between the equivalent system stiffness and initial GS pressure, when the geometric dimensions of the ICE are designed as shown above and its initial pressure  $p_0 = 0.125$  MPa. The corresponding compression ratio is 13:1. It is obvious that the equivalent system stiffness is almost proportional to the initial GS pressure  $p_{g0}$ .

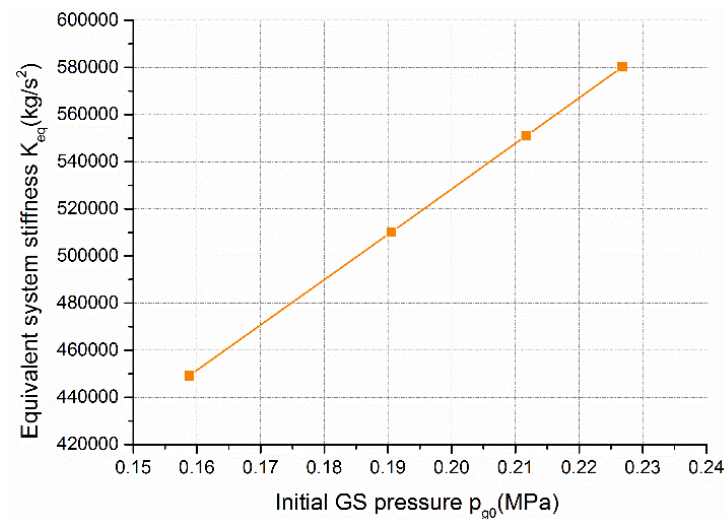


Figure 9. The equivalent system stiffness versus initial GS pressure.

Figure 10 depicts that the key operational parameters, like the initial GS pressure, motion frequency and equivalent system stiffness, increase almost linearly with the increasing of the objective output power. Meanwhile, the moving mass must be reduced accordingly.

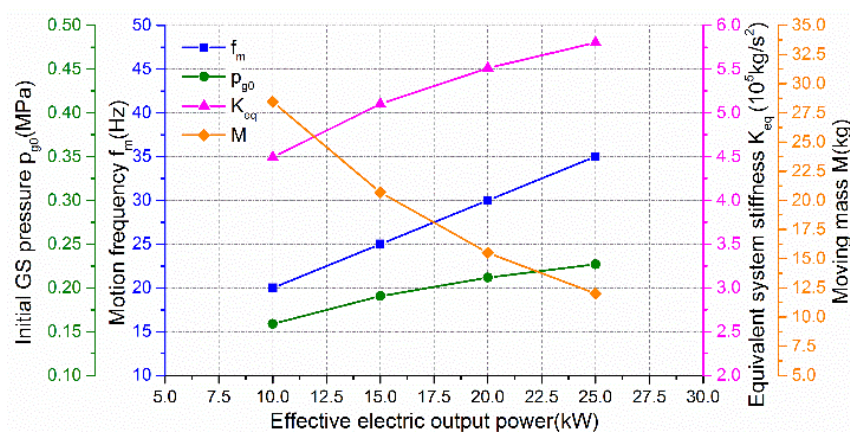


Figure 10. Operational parameters versus effective electric output power map.

As the motion frequency is 35 Hz, from (26)–(31), we can calculate that the moving mass is 12 kg theoretically, which is the total mass including the LEM mover, the ICE piston, the GS piston and the connecting devices. Considering this, the mass of the LEM mover must be designed less than 12 kg and the lighter the better. The equilibrium position is  $x_0 = 44.5$  mm. The equivalent system stiffness is 580,240 kg/s<sup>2</sup>. The critical starting position  $x_{sta}$  is defined at 85 mm, and the essential starting force is about 2853 N.

The LEM in this work is specially designed, as shown in Figure 11. In order to improve the electric power production capability, two linear electric machine units are assembled symmetrically. Each LEM unit is a 3-phase 21-pole/18-slot flat double-sided moving-magnet Permanent Magnet Synchronous Linear Machine (PMSLM) with Halbach magnet arrays, as shown in Figure 12. The left and right movers are connected with a middle keel beam, which is supported by a slide guide rail. Two guide rails are also assembled symmetrically on both sides of the mover plate. The mass of the LEM mover is less than 8.5 kg, and it can be further reduced by utilizing the special materials like the carbon fiber. The force constant is 150 N/A. And the line-to-line back electromotive force (EMF) coefficient is 87 V/ms<sup>-1</sup>.

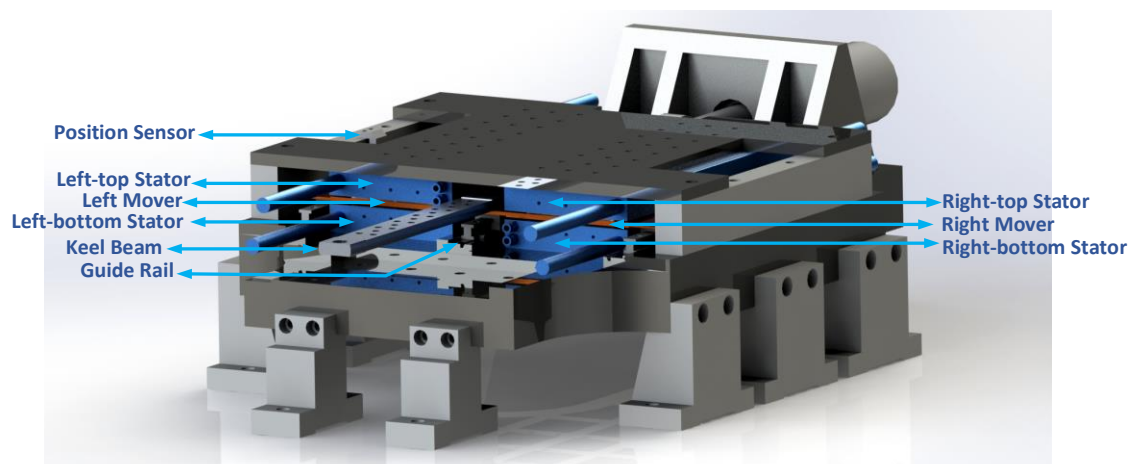


Figure 11. The 3D structure illustration of the linear electric machine.

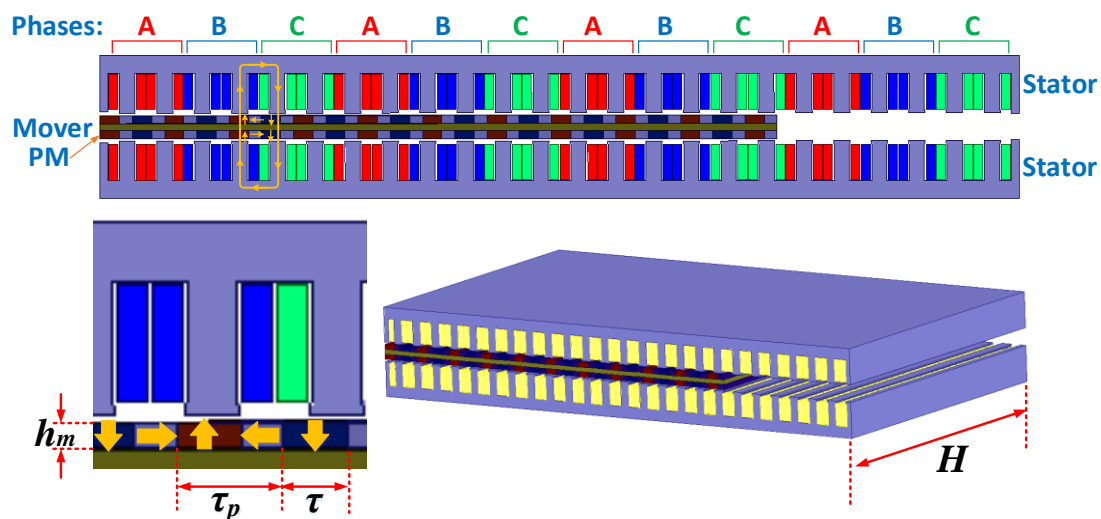


Figure 12. Axial cross-section 2D diagram and flux lines of the PMSLM.

The LEM is a notable component for the free-piston linear generator (FPLG) system. It is directly integrated between the internal combustion chamber and a rebounding device like a gas spring. In regards of the HEVs applications, the linear electrical generator is a core device that converts the mechanical energy of the piston-rod into electrical energy, and directly outputs to the load. Its performances has significant effects on the overall system performances. Besides, the electromagnetic force of the linear electrical generator determines the piston motion. The dynamic behavior of the piston-rod is highly dependent upon the mechanical-electrical response time of the linear electric generator. In addition, the LEM plays an important role in FPLG system, which requires that the LEM can not only run as a starting motor, but also a generator. Therefore, design an appropriate electrical generator solution specifically for FPLG system makes great sense [15,43,48].

The detailed LEM design process is not the key subject of this paper, therefore we simply provide the major structural parameters and performance specifications, which are listed in Table 6, where  $\eta_g$  is the generating efficiency,  $L_s$  is the winding inductance,  $R_s$  is the phase winding resistance,  $L_d$  and  $L_q$  are respectively d-axis and q-axis inductance,  $\psi_f$  is the PM flux,  $N$  is the number of winding turns per phase,  $\tau_p$  is the pole pitch,  $g_e$  is the effective air gap length,  $\tau$  and  $h_m$  are the width and thickness of PM,  $H_c$  is the coercive force of PM,  $B_m$  is the maximum air gap magnetic density,  $H$  is the stator width.

Table 6. LEM specifications.

Nominal	Value	Nominal	Value	Nominal	Value
$\eta_g$	94%	$L_s$	0.67 mH	$R_s$	0.16 $\Omega$
$L_d$	0.69 mH	$L_q$	0.69 mH	$\psi_f$	0.37 Wb
$N$	80	$\tau$	30 mm	$g_e$	33 mm
$\tau_p$	50 mm	$h_m$	12 mm	$H_c$	960 A/mm
$B_m$	0.83 T	$H$	300 mm		

### 3. Feasibility Verification of the Decoupling Design

Simulation and analysis are conducted to verify the feasibility of the proposed decoupling design approach. Because the focus of this manuscript is the proposed decoupling design approach and its validation, rather than the modeling of the coupling system, here, the simulation model is simply established based on the typical thermodynamics model of a free-piston linear generator that was reported in references [34,37,46,47,49], of which the feasibility was already validated with test data. The accuracy of the coupling thermodynamics model of the FPLG system is mainly depended on the accuracy of the free-piston ICE model. In order to describe the in-cylinder combustion process, we take the advantage of the Weiber combustion function [34,37,46,47,49], of which the accuracy is also validated with test data as reported in references [34,37].

The thermodynamics model of the coupling system is implemented and sub-models of the LEM, ICE and GS are engaged with the considerations of various operational states including the starting, stable operating, fault recovering and stopping processes. Figure 13 illustrates the diagram of the coupling simulation model developed with Matlab/Simulink. Table 7 lists the key simulation conditions specifically for the designed 25 kW FPLG system.

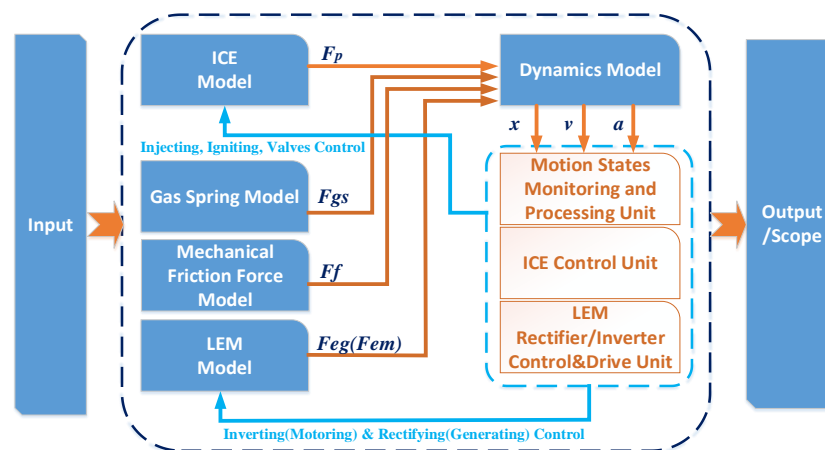
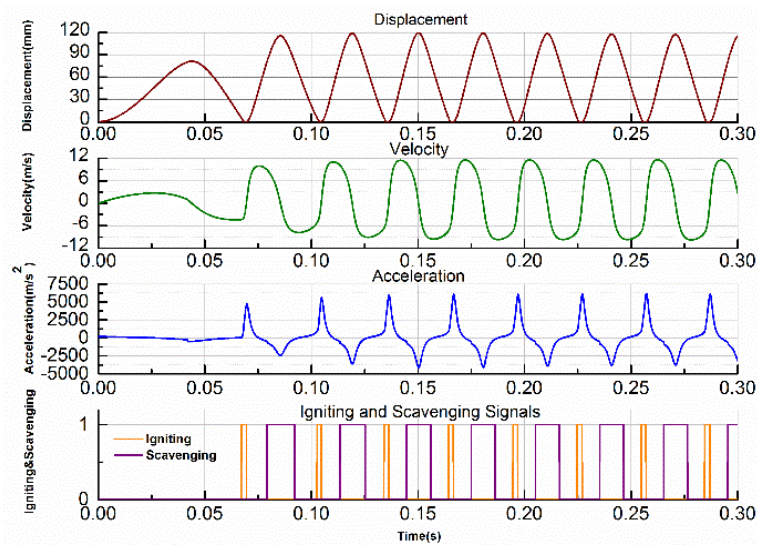


Figure 13. Simulation model diagram.

Table 7. Crucial simulation conditions.

Nominal	Value	Nominal	Value	Nominal	Value
$M$	11.9 kg	$g_f$	45 mg	$p_0$	0.125 MPa
$p_{g0}$	0.23000 MPa	$F_{EM}$	2853 N	$B_v$	12 N/ms <sup>-1</sup>

Figures 14 and 15 show that the FPLG designed with the decoupling design approach can run stably. Figure 14 shows the dynamic responses. Because the equivalent stiffness profiles of ICE and GS are different, during expansion-generating stroke and compression-generating stroke, the motion profile is not symmetrical.



**Figure 14.** Simulated dynamic responses (Displacement, velocity, acceleration, igniting and scavenging signals).

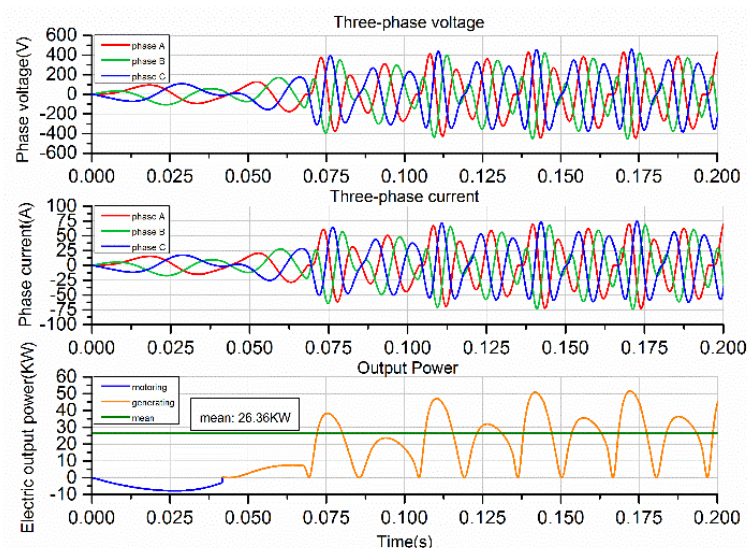


**Figure 15.** Three-phase voltage, current and electric power output.

The maximum displacement is 119.6 mm, and the equivalent compression ratio is 12.96. Here, the maximum compression ratio is simply a nominal value which is mainly limited by the designed stroke length and the combustion clearance of the combustion chamber. It is variable with different power demands and injected fuel mass per cycle. It also depends upon the choice of fuel. In general, the limitation of compression ratio lies in the fuel quality and its knock (self-ignition) characteristics, and is commonly between 7:1 and 11:1 for ordinary gasoline fuels. However, for leaner mixtures, the knock limit increases drastically, and may exceed a compression ratio of 15:1 for very lean mixtures [27]. The maximum velocity of the expansion-generating stroke is about 12 m/s, which is close to the design expectation, while in a compression-generating stroke, it is about 10 m/s, which is a little more than the design expectation. When the piston arrives at the predefined ignition position  $x_{ign} = 5$  mm, the ignition signal is enabled. When it reaches the predefined scavenging position  $x_{sca} = 85$  mm, the scavenging signal is enabled. After the moment of ignition, the acceleration increases dramatically, and can even reach about  $6250 \text{ m/s}^2$ . The average cycle duration is 29.4 ms. The simulated motion frequency  $f_m$  is about 34.01 Hz.

Figure 15 shows the electric power output profiles from starting phase to stable operation. With a constant initial motoring force of 2853 N, the designed FPLG can be started successfully after 68.75 ms. It also verifies that the designed system can run stably.

Because the velocity of the expansion process is larger than that of the compression process, the output electrical power during the expansion-generating stroke is thus larger than that during the compression-generating stroke. The simulated duration of the expansion is less than that of the compression stroke. The velocity in the compression stroke is large than that has been predefined in the decoupling process. That causes the final simulation difference factor  $k$  is less than 3, which is less than the predefined value. The maximum electrical power output is 52.57 kW and the average power is 26.36 kW, and the overall system efficiency is 36.32%.

As shown in Table 8, both the power and efficiency satisfy the design objectives. Besides, the simulated operational parameters such as the motion frequency, moving mass, fuel mass injected per cycle and the initial GS pressure accord well with the theoretical values. All errors of these operational parameters are less than 3%. This validates that the proposed decoupling design approach and the determination methodologies of the operational parameters are feasible.

**Table 8.** Objective and simulated specifications.

Nominal	Objective/Theoretical	Simulated	Error
$\eta_{eff}$	35.5%	36.32%	2.31%
$P_E$	25 kW	26.36 kW	5.16%
$f_m$	35 Hz	34.01 Hz	2.82%
$M$	12 kg	11.9 kg	0.83%
$g_f$	45.73 mg	45 mg	1.60%
$p_{g0}$	0.22681 MPa	0.23000 MPa	1.41%

As stated above, the designed FPLG is capable of providing over 25 kW effective electrical power with an overall minimum efficiency of 36.32%. In order to further state that such design is not an accidental success, several designs for different power specifications have been verified.

The major structural parameters remain the same as the abovementioned design, except for the fact the motion frequency, moving mass, injected fuel mass and initial GS pressure are changed with different output power demands. The corresponding results and comparisons are listed in Table 9. Accordingly, the results determined theoretically and that obtained from the simulation are compared in Figures 16–18.

**Table 9.** Verification and comparison for variable working conditions.

Objective Specifications	Nominal	$\eta_{eff}$ (%)	$P_E$ (kW)	$f_m$ (Hz)	$M$ (kg)	$g_f$ (mg)	$p_{g0}$ (MPa)
10 kW (20 Hz)	Theoretical	35.50	10.00	20	28.4	32.01	0.15877
	Simulated	37.36	10.26	19.82	28	31.5	0.1625
	Error	-	-	0.90%	1.41%	1.60%	2.35%
15 kW (25 Hz)	Theoretical	35.50	15.00	25	20.7	38.41	0.19052
	Simulated	38.92	15.55	24.88	20	36.5	0.19805
	Error	-	-	0.48%	3.38%	4.97%	3.95%
20 kW (30 Hz)	Theoretical	35.50	20	30	15.5	42.68	0.21169
	Simulated	40.06	21.19	29.5	15	40.75	0.22000
	Error	-	-	1.67%	3.33%	4.52%	3.93%
25 kW (35 Hz)	Theoretical	35.50	25	35	12	45.73	0.22681
	Simulated	36.32	26.36	34.01	11.9	45.00	0.23000
	Error	-	-	2.82%	0.83%	1.60%	1.41%

Figure 16 shows that, for different output powers like 10 kW, 15 kW, 20 kW and 25 kW, all the practical power and efficiency are larger than that of the objectives. It proves that the proposed decoupling design approach is feasible for different power levels under certain overall efficiency demand. It also states that the above-designed FPLG can generate various power through adjusting the operational parameters.

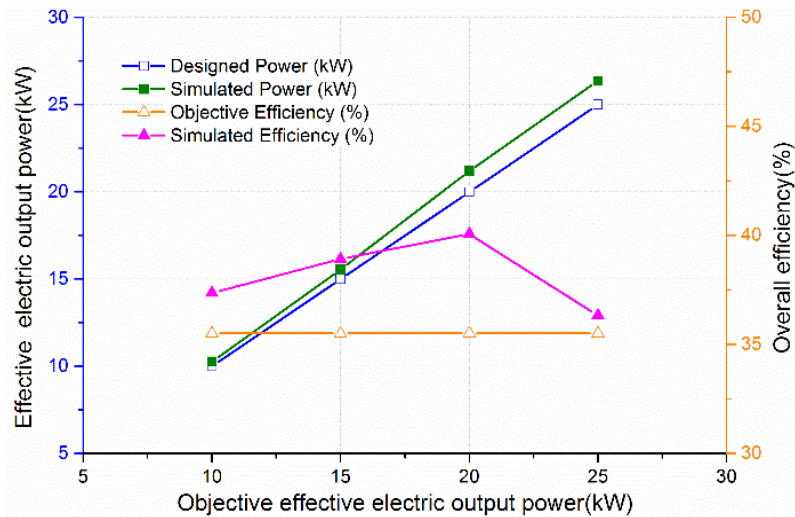


Figure 16. Power and efficiency comparison for various power demands.

Figure 17 shows the comparison between the theoretical and simulated operational parameters for various power demands. The simulated values of the moving mass, motion frequency, injected fuel mass and initial GS pressure accord well with the theoretical values, and the corresponding errors are all below 5%, as shown in Figure 18.

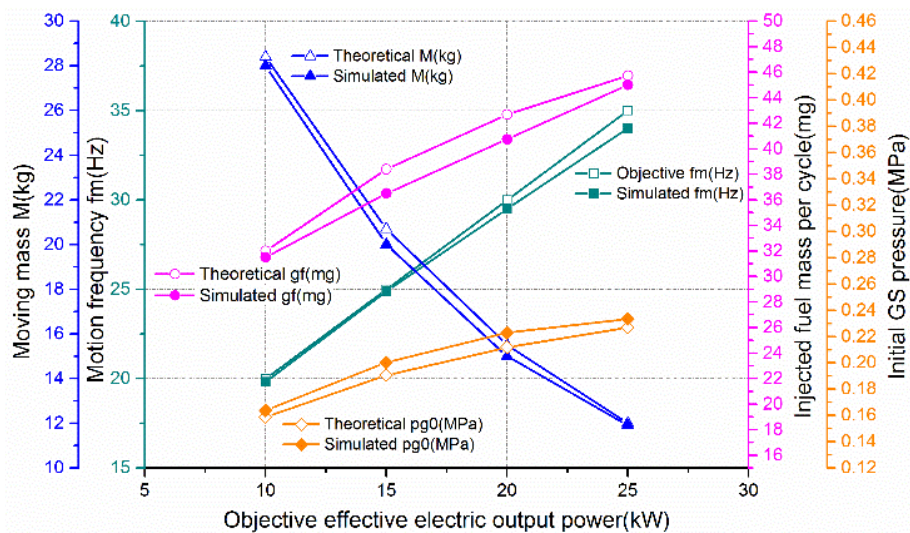


Figure 17. Comparisons of the theoretical and simulated operational parameters for various power demands.

It shows that the theoretical determinations of the key operational parameters are practicable, which again validates the feasibility of the proposed decoupling design approach, when, gasoline is utilized as the fuel (calorific value is 44,000 J/g) for a two-stroke single-cylinder FPLG.

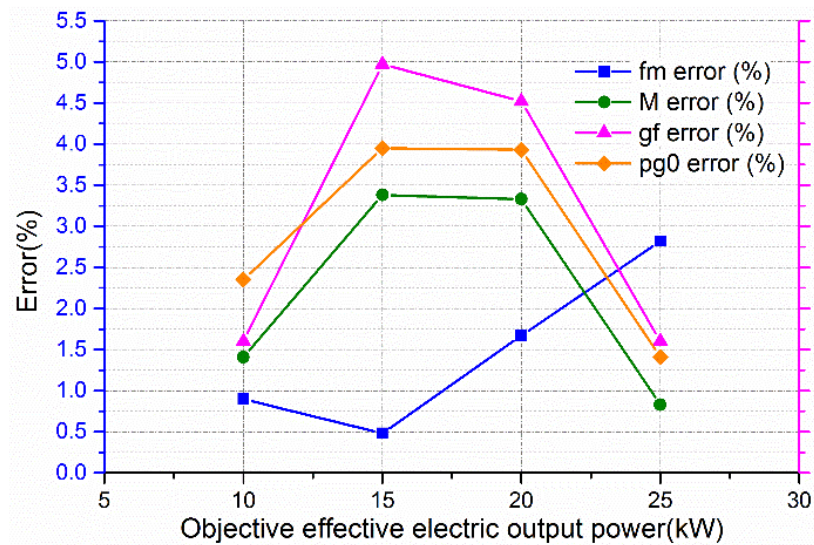


Figure 18. Errors of the key operational parameters for various power demands.

#### 4. Conclusions

This paper has focused on the design of the FPLG system. A decoupling design concept based on the distribution theory of energy, power and efficiency has been proposed specifically for single-cylinder gas spring rebounded FPLG. The theoretical design approach has provided an effective design guideline directly from the objective power and efficiency demands. It has also presented the methodology of determining the key geometrical and operational parameters.

The feasibility of the proposed decoupling design approach has been verified through several design examples with different output power specifications like 10, 15, 20 and 25 kW. The simulated power and efficiency are all larger than the design objectives with over 35.5% total system efficiency. The design examples have validated that the key operational parameters accord well with their theoretical determinations, with errors below 5%.

Further investigations of the coupling dynamics of the designed FPLG are necessary. The detailed coupling dynamics modeling and analysis with crucial control strategies under different operational conditions will be conducted in the subsequent works.

**Acknowledgments:** This work is supported by the International S&T Cooperation Projects of China (Grant No. 2014DFA71010); One Hundred Talents Program of the Chinese Academy of Sciences; Natural Science Foundation of Ningbo (No. 2015A610146 & No. 2015A610154). We would like to thank the sponsors.

**Author Contributions:** Peng Sun completed most of the theoretical derivation, system modeling and simulation analysis, and finished this manuscript; Chi Zhang provided the ideas of the design methods and inspiration of the decoupling design approach, also contributed significantly to enhance the manuscript; Jinhua Chen completed part of the design analysis of the electrical machine; Fei Zhao provided the configuration design instructions of the FPLG; Youyong Liao was responsible for part of the system design and simulation analysis; Guilin Yang also provided the ideas of the decoupling design based on the energy distribution theory, and also contributed significantly to the enhance of the manuscript; Chinyin Chen designed the structure of the system and also contributed significantly to the enhance of the manuscript.

**Conflicts of Interest:** The authors declare no conflict of interest.

#### Nomenclature

$P_E$	effective overall output electric power (kW)
$T_{cyc}$	piston motion cycle duration (s)
$f_m$	piston motion frequency (Hz)
$M$	mass of piston rod (kg)
$K_{eq}$	system equivalent stiffness (kg/s <sup>2</sup> )
$D$	cylinder bore of combustion chamber (m)

$S$	stroke length (m)
$S_c$	combustion clearance space (m)
$V_c$	effective combustion clearance the ICE (m)
$V_s$	discharge capacity of the ICE (cc)
$V$	combustion chamber instantaneous volume ( $m^3$ )
$D_g$	cylinder bore of gas spring (m)
$S_g$	piston stroke length of gas spring (m)
$S_{cg}$	clearance space of gas spring (m)
$V_g$	instantaneous working volume of gas spring ( $m^3$ )
$n_{crank}$	equivalent crankshaft speed (rpm)
$N_{strokes}$	number of strokes
$N_{cylinder}$	number of cylinders
$\chi_B$	mass fraction burned in the combustion process
$g_f$	injected fuel mass per cycle (mg/cycle)
$H_u$	calorific value of fuel (J/g)
$F_{Em}$	minimum effective motoring force (N)
$K_{eq}$	system equivalent stiffness ( $kg/s^2$ )
$v_s$	piston velocity at the starting position (m/s)
$B_v$	friction coefficient ( $N/ms^{-1}$ )
$x_0$	equilibrium position (m)
$\epsilon_0$	objective compression ratio
$\gamma$	polytropic exponent
$A_g$	effective cross-sectional area of GS piston ( $m^2$ )
$Q_0$	total chemical energy of the fuel in cylinder (J)
$Q_B$	combustion released energy (J)
$W_e$	piston effective mechanical energy output (J)
$Q_{Ec}$	output electric energy during compression-generating stroke (J)
$Q_{Ee}$	output electric energy during expansion-generating stroke (J)
$Q_{Le}$	energy loss in the expansion-generating stroke (J)
$Q_{Lc}$	energy loss in the compression-generating stroke (J)
$\Delta Q_{GS}$	energy stored in GS during expansion-generating stroke (J)
$\eta_1$	expansion-generating efficiency
$\eta_2$	compression-generating efficiency
$\eta_c$	combustion efficiency
$\eta_g$	LEM generating efficiency
$\eta_{eff}$	effective overall system efficiency
$P_{ele}$	instantaneous electric power generation (kW)
$P_E$	effective electric power generation (kW)
$P_{me}$	effective mechanical output power of ICE (kW)
$p_0$	initial in-cylinder pressure (MPa)
$p_{me}$	mean effective in-cylinder pressure (MPa)
$p$	pressure in combustion chamber (MPa)
$p_g$	pressure in gas spring chamber (MPa)
$p_{g0}$	initial pressure of gas spring (MPa)
$p_{meg}$	mean effective pressure in gas spring chamber (MPa)
$\Delta W_p$	work done by the ICE on the piston (J)
$\Delta W_{pg}$	work done by the gas spring on the piston (J)
$\Delta W_f$	friction loss energy (J)
$\Delta W_k$	starting kinetic energy of the piston (J)
$V_{gT}$	volume of GS chamber when piston at TDC position ( $m^3$ )
$V_{gB}$	volume of GS chamber when piston at BDC position ( $m^3$ )
$A$	effective cross-sectional area of ICE piston ( $m^2$ )
$x_{ign}$	ignition position
$x_{sta}$	critical starting position
$x_{inj}$	injection position
$x_{sca}$	scavenging position
IVO	intake valve open
IVC	intake valve close
EVO	exhaust valve open
EVC	exhaust valve close
IGS	ignition start

## References

1. Mikalsen, R.; Roskilly, A.P. A review of free-piston engine history and applications. *Appl. Therm. Eng.* **2007**, *27*, 2339–2352. [[CrossRef](#)]
2. Schneider, S.; Rinderknecht, F. A high efficient energy converter with flex fuel potential. In Proceedings of the 2013 International Conference on Clean Electrical Power (ICCEP), Alghero, Italy, 11–13 June 2013; pp. 453–460.
3. Heron, A.; Rinderknecht, F. Comparison of range extender technologies for battery electric vehicles. In Proceedings of the 2013 8th International Conference and Exhibition on Ecological Vehicles and Renewable Energies (EVER), Monte Carlo, Monaco, 27–30 March 2013; pp. 1–6.
4. Cornelius, H.E.F. *Development of a Free-Piston Linear Generator for Use in an Extended Range Electric Vehicle*; EVS26: Los Angeles, CA, USA, 2012.
5. Cawthorne, W.R.; Famouri, P.; Chen, J.; Clark, N.N.; McDaniel, T.I.; Atkinson, R.J.; Nandkumar, S.; Atkinson, C.M.; Petreanu, S. Development of a linear alternator-engine for hybrid electric vehicle applications. *IEEE Trans. Veh. Technol.* **1999**, *48*, 1797–1802. [[CrossRef](#)]
6. Mikalsen, R.; Roskilly, A.P. The control of a free-piston engine generator. Part 1: Fundamental analyses. *Appl. Energy* **2010**, *87*, 1273–1280. [[CrossRef](#)]
7. Rinderknecht, F.; Kock, F. A High Efficient Energy Converter for a Hybrid Vehicle Concept-Gas Spring Focused. In Proceedings of the Symposium EVER12, Monte Carlo, Monaco, 22–24 March 2012.
8. Kock, F.; Haag, J.; Friedrich, H.E. The Free Piston Linear Generator-Development of an Innovative, Compact, Highly Efficient Range-Extender Module. *SAE Tech. Pap.* **2013**. [[CrossRef](#)]
9. Ferrari, C.; Friedrich, H.E. Development of a free-piston linear generator for use in an extended-range electric vehicle. In Proceedings of the EVS26 International Battery, Hybrid and Fuel Cell Electric Vehicle Symposium, Los Angeles, CA, USA, 6–9 May 2012.
10. Schneider, S.; Rinderknecht, F.; Friedrich, H.E. Design of future concepts and variants of The Free Piston Linear Generator. In Proceedings of the 2014 Ninth International Conference on Ecological Vehicles and Renewable Energies (EVER), Monte Carlo, Monaco, 25–27 March 2014; pp. 1–8.
11. Kosaka, H.; Akita, T.; Moriya, K.; Goto, S.; Hotta, Y.; Umeno, T.; Nakakita, K. Development of Free Piston Engine Linear Generator System Part 1—Investigation of Fundamental Characteristics. *SAE Tech. Pap.* **2014**. [[CrossRef](#)]
12. Goto, S.; Moriya, K.; Kosaka, H.; Akita, T.; Hotta, Y.; Umeno, T.; Nakakita, K. Development of Free Piston Engine Linear Generator System Part 2—Investigation of Control System for Generator. *SAE Tech. Pap.* **2014**. [[CrossRef](#)]
13. Jiming, L.; Siqin, C. Modeling and simulation of a novel internal combustion-linear generator integrated power system using Matlab/Simulink. In Proceedings of the 2012 IEEE International Conference on Power and Energy (PECon), Kota Kinab, Malaysia, 2–5 December 2012; pp. 435–439.
14. Xu, Z.; Chang, S. Prototype testing and analysis of a novel internal combustion linear generator integrated power system. *Appl. Energy* **2010**, *87*, 1342–1348. [[CrossRef](#)]
15. Zheng, P.; Chen, A.; Thelin, P.; Arshad, W.M.; Sadarangani, C. Research on a tubular longitudinal flux PM linear generator used for free-piston energy converter. *IEEE Trans. Magn.* **2007**, *43*, 447–449. [[CrossRef](#)]
16. Hansson, J.; Leksell, M. Performance of a series hybrid electric vehicle with a free-piston energy converter. In Proceedings of the Vehicle Power and Propulsion Conference, Windsor, UK, 6–8 September 2006; pp. 1–6.
17. Hansson, J.; Leksell, M.; Carlsson, F.; Sadarangani, C. Operational strategies for a free piston energy converter. In Proceedings of the Fifth International Symposium on Linear Drives for Industry Applications, Kobe-Awaji, Japan, 25–28 September 2005.
18. Khayyer, P.; Famouri, P. Application of Two Fuel Cells in Hybrid Electric Vehicles. *SAE Tech. Pap.* **2008**. [[CrossRef](#)]
19. Shoukry, E.F. *Numerical Simulation for Parametric Study of a Two-Stroke Compression Ignition Direct Injection Linear Engine*; West Virginia University: Morgantown, WV, USA, 2003.
20. Shoukry, E.; Taylor, S.; Clark, N.; Famouri, P. Numerical Simulation for Parametric Study of a Two-Stroke Direct Injection Linear Engine. *SAE Tech. Pap.* **2002**. [[CrossRef](#)]
21. Xiao, J.; Li, Q.; Huang, Z. Motion characteristic of a free piston linear engine. *Appl. Energy* **2010**, *87*, 1288–1294. [[CrossRef](#)]

22. Hanipah, M.R.; Mikalsen, R.; Roskilly, A. Recent commercial free-piston engine developments for automotive applications. *Appl. Therm. Eng.* **2015**, *75*, 493–503. [[CrossRef](#)]
23. Mikalsen, R.; Roskilly, A.P. The control of a free-piston engine generator. Part 2: Engine dynamics and piston motion control. *Appl. Energy* **2010**, *87*, 1281–1287. [[CrossRef](#)]
24. Mikalsen, R.; Jones, E.; Roskilly, A.P. Predictive piston motion control in a free-piston internal combustion engine. *Appl. Energy* **2010**, *87*, 1722–1728. [[CrossRef](#)]
25. Mikalsen, R.; Roskilly, A.P. A computational study of free-piston diesel engine combustion. *Appl. Energy* **2009**, *86*, 1136–1143. [[CrossRef](#)]
26. Mikalsen, R.; Roskilly, A.P. Coupled dynamic–multidimensional modelling of free-piston engine combustion. *Appl. Energy* **2009**, *86*, 89–95. [[CrossRef](#)]
27. Mikalsen, R.; Roskilly, A.P. Performance simulation of a spark ignited free-piston engine generator. *Appl. Therm. Eng.* **2008**, *28*, 1726–1733. [[CrossRef](#)]
28. Mikalsen, R.; Roskilly, A. The design and simulation of a two-stroke free-piston compression ignition engine for electrical power generation. *Appl. Therm. Eng.* **2008**, *28*, 589–600. [[CrossRef](#)]
29. Miao, Y.; Zuo, Z.; Feng, H.; Guo, C.; Song, Y.; Jia, B.; Guo, Y. Research on the Combustion Characteristics of a Free-Piston Gasoline Engine Linear Generator during the Stable Generating Process. *Energies* **2016**, *9*, 655. [[CrossRef](#)]
30. Feng, H.; Guo, Y.; Song, Y.; Guo, C.; Zuo, Z. Study of the Injection Control Strategies of a Compression Ignition Free Piston Engine Linear Generator in a One-Stroke Starting Process. *Energies* **2016**, *9*, 453. [[CrossRef](#)]
31. Feng, H.; Song, Y.; Zuo, Z.; Shang, J.; Wang, Y.; Roskilly, A. Stable Operation and Electricity Generating Characteristics of a Single-Cylinder Free Piston Engine Linear Generator: Simulation and Experiments. *Energies* **2015**, *8*, 765–785. [[CrossRef](#)]
32. Jia, B.; Smallbone, A.; Zuo, Z.; Feng, H.; Roskilly, A.P. Design and simulation of a two- or four-stroke free-piston engine generator for range extender applications. *Energy Convers. Manag.* **2016**, *111*, 289–298. [[CrossRef](#)]
33. Jia, B.; Smallbone, A.; Feng, H.; Tian, G.; Zuo, Z.; Roskilly, A.P. A fast response free-piston engine generator numerical model for control applications. *Appl. Energy* **2016**, *162*, 321–329. [[CrossRef](#)]
34. Feng, H.; Guo, C.; Yuan, C.; Guo, Y.; Zuo, Z.; Roskilly, A.P.; Jia, B. Research on combustion process of a free piston diesel linear generator. *Appl. Energy* **2016**, *161*, 395–403. [[CrossRef](#)]
35. Zhang, S.; Zhao, C.; Zhao, Z.; Ma, F. Combustion characteristics analysis of hydraulic free piston diesel engine. *Appl. Energy* **2015**, *160*, 761–768. [[CrossRef](#)]
36. Zhang, S.; Zhao, C.; Zhao, Z. Stability analysis of hydraulic free piston engine. *Appl. Energy* **2015**, *157*, 805–813. [[CrossRef](#)]
37. Jia, B.; Zuo, Z.; Tian, G.; Feng, H.; Roskilly, A.P. Development and validation of a free-piston engine generator numerical model. *Energy Convers. Manag.* **2015**, *91*, 333–341. [[CrossRef](#)]
38. Jia, B.; Tian, G.; Feng, H.; Zuo, Z.; Roskilly, A.P. An experimental investigation into the starting process of free-piston engine generator. *Appl. Energy* **2015**, *157*, 798–804. [[CrossRef](#)]
39. Johnson, T. *Free-Piston Engine*; Sandia National Laboratories: Albuquerque, NM, USA, 2012.
40. Van Blarigan, P. Free-Piston Engine; Transportation Energy Center Center. In Proceedings of the 2009 DOE Vehicle Technologies Program Annual Merit Review, Arlington, VA, USA; pp. 1–17.
41. Mao, J.; Zuo, Z.; Feng, H. Parameters coupling designation of diesel free-piston linear alternator. *Appl. Energy* **2011**, *88*, 4577–4589. [[CrossRef](#)]
42. Kleemann, A.; Dabadie, J.-C.; Henriot, S. Computational Design Studies for a High-Efficiency and Low-Emissions Free Piston Engine Prototype. *SAE Tech. Pap.* **2004**. [[CrossRef](#)]
43. Arshad, W.M.; Sadarangani, C.; Bäckström, T.; Thelin, P. Finding an appropriate electrical machine for a free piston generator. In Proceedings of the 19th Electrical Vehicle Symposium (EVS), Busan, Korea, 19–23 October 2002; pp. 427–437.
44. Wang, J.; West, M.; Howe, D.; la Parra, H.-D.; Arshad, W.M. Design and experimental verification of a linear permanent magnet generator for a free-piston energy converter. *IEEE Trans. Energy Convers.* **2007**, *22*, 299–306. [[CrossRef](#)]
45. Heywood, J.B. *Internal Combustion Engine Fundamentals*; Automotive Technology Series; McGraw-hill: New York, NY, USA, 1988; p. 723.

46. Atkinson, C.M.; Petreanu, S.; Clark, N.N.; Atkinson, R.J.; McDaniel, T.I.; Nandkumar, S.; Famori, P. Numerical Simulation of a Two-Stroke Linear Engine-Alternator Combination. *SAE Tech. Pap.* **1999**. [[CrossRef](#)]
47. Kim, J.; Bae, C.; Kim, G. Simulation on the effect of the combustion parameters on the piston dynamics and engine performance using the Wiebe function in a free piston engine. *Appl. Energy* **2013**, *107*, 446–455. [[CrossRef](#)]
48. Rinderknecht, F. A highly efficient energy converter for a hybrid vehicle concept-focused on the linear generator of the next generation. In Proceedings of the 2013 8th International Conference and Exhibition on Ecological Vehicles and Renewable Energies (EVER), Monte Carlo, Monaco, 27–30 March 2013; pp. 1–7.
49. Mao, J.; Zuo, Z.; Li, W.; Feng, H. Multi-dimensional scavenging analysis of a free-piston linear alternator based on numerical simulation. *Appl. Energy* **2011**, *88*, 1140–1152. [[CrossRef](#)]



© 2016 by the authors; licensee MDPI, Basel, Switzerland. This article is an open access article distributed under the terms and conditions of the Creative Commons Attribution (CC-BY) license (<http://creativecommons.org/licenses/by/4.0/>).